JOURNAL OF THERMOPHYSICS AND HEAT TRANSFER
Vol. 23, No. 3, July–September 2009

Partially Confined FC-72 Spray-Cooling Performance: Effect of Dissolved Air

Rebekah L. Puterbaugh* and Kirk L. Yerkes†
U.S. Air Force Research Laboratory, Wright–Patterson Air Force Base, Ohio 45433
and
Scott K. Thomas‡
Wright State University, Dayton, Ohio 45435

DOI: 10.2514/1.41654

The objective of this paper was to investigate the heat transfer performance of a partially confined FC-72 spray with varying dissolved-air concentrations. An experimental test rig consisting of a spray chamber coupled to a fluid-delivery-loop system was used to obtain temperature, pressure, and critical heat flux data. A downward-facing nozzle within the spray chamber allowed the FC-72 fluid to be sprayed onto an upward-facing thick-film resistor heater. The heater was mounted onto a glass post, with a sump system to allow removal of excess fluid. Type-E thermocouples were embedded in the post to obtain temperature data. The parametric ranges for experimental testing were as follows: volume-percent concentration of dissolved air was $5 \le C_m \le 18\%$, chamber pressure was $6.90 \times 10^4 \le P_{ch} \le 8.27 \times 10^4$ N/m^2 ($10 \le P_{ch} \le 12$ psia), liquid subcooling was $2 \le \Delta T_{sc} \le 12$°C, and volumetric flow rate was $6.31 \le \dot{V} \le 10.5$ cm^3/s ($6.0 \le \dot{V} \le 10.0$ gph). Test data were obtained for comparison of critical heat flux with varying C while controlling the spray chamber pressure. The applicability of Henry's law to the current system was investigated, and air concentration measurements using Henry's law were compared with those obtained using a direct sample method. An empirical mathematical relationship allowing for determination of surface heat flux with varying flow rate was also developed. The relationship was obtained using test data at flow rates of $\dot{V} = 6.31$, 8.41, and 10.5 cm^3/s and was validated using experimental data obtained for flow rates of $\dot{V} = 7.36$ and 9.46 cm^3/s (7.0 and 9.0 gph).

Nomenclature

A	=	area, m^2
a	=	acceleration level, g
C	=	percent air content by volume, $[V_{air}/(V_{FC} + V_{air})] \times 100$
C^*	=	air volume ratio, V_{air}/V_{FC}
D	=	droplet diameter, m
Fr	=	Froude number, v^2/aD
f	=	heater conduction loss fraction
Ga	=	Galileo number, $aD^3\rho^2/\mu^2$
H	=	Henry's constant, mol/mol · kPa
h	=	heat transfer coefficient, W/(m^2 − K)
k	=	thermal conductivity, W/(m − K)
M	=	molar fraction, $N_{air}/(N_{FC} + N_{air})$
M^*	=	molar ratio, N_{air}/N_{FC}
m	=	molar mass, g/mol
$\dot{m}''$	=	mass flow rate per unit area, kg/(m^2 · s)
N	=	number of moles
P	=	pressure, N/m^2
P_g	=	partial pressure, N/m^2
Q	=	heat rate, W
q	=	heat flux, W/m^2
T	=	temperature, K
t	=	time, s
V	=	volume, m^3
$\dot{V}$	=	volumetric flow rate, m^3/s
$\dot{V}''$	=	volumetric flow rate per unit area, m^3/(m^2 · s)
Z	=	thickness, m
ΔT	=	wall superheat, $T_s - T_{sat}$, K
ΔT_{sc}	=	fluid subcooling, $T_f - T_{sat}$, K
μ	=	absolute viscosity, kg/m · s
v	=	droplet velocity, m/s
ρ	=	density, kg/m^3
σ	=	surface tension, kg/s^2

Subscripts

CHF	=	critical heat flux
ch	=	chamber
cov	=	heater glass cover plate
FC	=	FC-72 fluid
htr	=	heater conductive layer
int	=	interface between heater substrate and insulating support post
m	=	measured
ref	=	reference value corresponding to rig conditions at time of fluid sample
s	=	heater surface
sat	=	saturation
sub	=	heater ceramic substrate

Received 16 October 2008; revision received 24 February 2009; accepted for publication 11 March 2009.

*Associate Mechanical Engineer, Propulsion Directorate, Turbine Engine Division, Engine Integration and Assessment Branch, 1950 Fifth Street. Member AIAA.

†Deputy for Science, Propulsion Directorate, Energy, Power and Thermal Division, 1950 Fifth Street. Associate Fellow AIAA.

‡Associate Professor, Department of Mechanical and Materials Engineering. Associate Fellow AIAA.

Introduction

ELECTRONIC devices are being packaged in smaller spaces, causing increasingly larger heat fluxes. Two-phase cooling can be extremely effective for high heat fluxes, because it takes advantage of the latent heat of vaporization. The boiling process has several regimes that occur as heat is transferred from a solid surface to a liquid in contact with that surface, such as free convection, nucleate boiling, transition boiling, and film boiling. Figure 1 shows a typical boiling curve for cooling liquids. The onset of nucleate boiling, or the

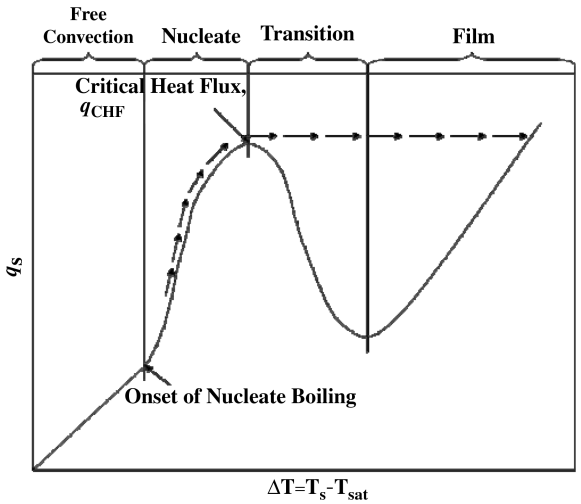

Fig. 1 Pool boiling regimes: surface heat flux versus wall superheat.

point at which bubbles start forming on the solid surface, is shown. Upon reaching critical heat flux, the point at which maximum heat transfer occurs, a sharp departure of the boiling curve occurs and the wall superheat increases dramatically. From the plot, it can be inferred that the optimal operating range for maximum heat transfer is just before reaching CHF. If CHF is exceeded, the surface temperature of the device being cooled will radically increase. In electronic devices, the onset of a CHF event followed by a sudden temperature spike could cause catastrophic failure. As a result, operating parameters for any two-phase cooling system for application to electronics must be fully investigated. An optimal operating window must be defined so that maximum heat transfer takes place without the risk of damage to the device as a result of reaching CHF.

Spray cooling has great potential in the area of electronics cooling, because the impact momentum of the droplets is low and the heat transfer rate achievable is high. To investigate spray cooling and its limitations in certain environments, a test rig was designed and built by Baysinger et al. [1] and was used by Baysinger [2] and Yerkes et al. [3] to perform further testing. Upon analysis of test results, a question was raised concerning possible effects of absorbed air in the FC-72 working fluid. It has been noted in previous research that the heat transfer associated with spray cooling is affected by the amount of dissolved air present in the cooling fluid. Although research has been conducted concerning this topic, the effect of dissolved air on spray-cooling efficiency has not been completely characterized.

The effect of dissolved air on spray cooling with water as the working fluid was investigated by Milke et al. [4]. A solid plate of glasslike material was heated using radiant heaters and spray-cooled using a droplet dispenser positioned vertically over the tile. An infrared camera was used to record the transient thermal behavior of the plate as the droplets were dispensed onto the surface and evaporated. Initial surface temperatures used in the experiment were $T_s = 110$, 130, 150, 160, and 180°C. Air-saturated deionized water was sprayed in a range of mass fluxes from $\dot{m}'' = 0.24$ to 1.6 g/(m$^2 \cdot$ s). Three varying mass fluxes were used for each initial temperature. The results from Milke et al.'s experiment were compared with results obtained in previous experiments involving degassed deionized water performed by Dawson and diMarzo [5]. For air-saturated water, as well as degassed water, the heated surface showed exponential cooling from the initial temperature to a steady-state temperature. In the experiments involving air-saturated water, however, a lower steady-state temperature was achieved than in those involving degassed water. To quantitatively compare the degassed and air-saturated results, the solid-surface temperature drop, along with a reference temperature, was examined. The reference temperature was defined as the difference between the solid-surface temperature at the onset of nucleate boiling for degassed water and the initial solid-surface temperature. The ratio of the surface temperature change to the reference temperature was examined for air-saturated and degassed water spray cooling. For large ratios, the air-saturated and degassed water had similar cooling effects on the heated surface. For smaller ratios, however, it was observed that dissolved gases in the water enhanced cooling. The actual amount of dissolved air in the fluid was not calculated or measured.

The effect of dissolved air on spray cooling with FC-72 was addressed by Lin and Ponnappan [6]. A plate containing eight miniature nozzles was used to spray cooling fluid over a surface area attached to a copper block heated by cartridge heaters. The nozzle array was used to investigate thermal performance data for various fluids, operating temperatures, nozzle pressure drops, and heat fluxes. To directly address the effect of dissolved air on the thermal performance of the system, FC-72 was used as one of the working fluids. A test was run using liquid that had been degassed, and another was run using liquid containing a certain unspecified amount of air. The degassing method for the liquid was not mentioned, but a difference in chamber pressure verified that the tests were run at differing air contents. The chamber pressure when using liquid containing air was $P_{ch} = 0.85$ bar, and the pressure when using degassed fluid was $P_{ch} = 0.295$ bar. The volumetric flow rate per unit cooling area onto the heated surface was between $\dot{V}'' = 0.019$ and 0.0205 m^3/(m$^2 \cdot$ s) for both tests. Results involving degassed fluid indicated better thermal performance than those with dissolved air up until CHF was reached. After reaching CHF, performance was better when dissolved air was present. The surface temperature was higher when dissolved air was present for $q < 70$ W/cm^2. For $q > 70$ W/cm^2, however, the surface temperature was lower when dissolved air was present. The amount of dissolved gas was not known.

Horacek et al. [7] investigated the effect of dissolved air on spray-cooling heat transfer using a full cone spray nozzle and microheater array. The test system was a closed flow loop including a spray chamber, condenser, and pump. The array consisted of 96 microheaters maintained at a specified constant temperature using 96 separate Wheatstone bridge feedback circuits. The flow rate through the spray nozzle was set at $\dot{V} = 37$ ml/ min (0.62 cm^3/s). Saturation temperatures varied from 25°C $\leq T_{sat} \leq$ 65°C. FC-72 was used as a test fluid, and the amount of dissolved air in the fluid was controlled by varying the pressure within the test section using a vacuum pump. Five test cases were conducted with varying air content and liquid subcooling. As the amount of dissolved air in the working fluid was increased, the overall spray-cooling efficiency was seen to increase when the five cases were compared. CHF levels ranged from approximately $40 \leq q_{CHF} \leq 65$ W/cm^2, increasing as the amount of air increased. The shift of the cooling curves to higher temperatures as air content increased was attributed to higher saturation temperatures. Other reasons for the effect of the dissolved air were proposed, such as possible additional single-phase convection of the heater areas not covered by droplets. It was also theorized that the air may cause bubble nucleation within the spray droplets, increasing the liquid–solid contact area or the liquid–vapor contact area. For the experiment, Henry's law was used to calculate the amount of dissolved air via partial pressure. Henry's law states that the solubility of a gas in a liquid at a given temperature is directly proportional to the partial pressure of the gas over the solution. For example, when the pressure exerted on a closed container with liquid and air inside is increased, the solubility of the air in the liquid is increased. Thus, the liquid in the container is forced to absorb more air.

Further work was done by Horacek et al. [8] to investigate the effect of dissolved air on spray-cooling heat transfer using measurements of time- and space-resolved heat transfer distributions and measurements of the liquid–solid contact area and three-phase contact line length. The experimental setup was similar to the previous experiment described, with the same flow loop and heaters. A high-speed digital camera was used to measure areas of liquid–solid contact through the semitransparent heater array using a total internal reflectance technique. As a result, the amount of area covered by liquid on the heater, along with the length of the three-phase contact line, could be determined using FC-72 as a cooling fluid. The flow rate through the spray nozzle was set at $\dot{V} = 32$ ml/ min

(0.53 cm^3/s). Liquid subcooling, or the temperature difference between the reservoir temperature and the liquid spray temperature, ranged from −1.5 to 21.1°C. Gas subcooling, or the difference between the saturation temperature and the reservoir temperature, ranged from 3.6 to 39.6°C. As with the previous experiment, the overall spray-cooling efficiency was seen to increase with increasing air content when five cases were compared. CHF levels ranged from approximately $50 \leq q_{CHF} \leq 65$ W/cm^2, increasing with the dissolved-air content. The results indicated that an increase in dissolved air within the fluid caused the saturation temperature of the fluid to increase, thereby increasing the subcooling of the fluid, which in turn caused an increase in heat transfer. Visualization of the spray indicated that increased air content in the fluid caused intermittent dry regions to appear on the heater in greater number and frequency than in cases when air was not present. A proposed reason for this was the mass transport of the absorbed air escaping the liquid as it was heated. As in the previous work, partial pressures were used to calculate the amount of dissolved air in the liquid.

The objective of the present investigation was to determine the effect of absorbed air on critical heat flux with FC-72 as the working fluid while controlling the spray chamber pressure. For the current experiment, 3M Fluorinert FC-72 was chosen as the working fluid because it is dielectric, noncorrosive, nontoxic, nonflammable, and inert. In contrast to previous research, the amount of dissolved air per unit volume was measured directly. Because amounts of air as large as 48% by volume can be dissolved in FC-72 [9], an understanding of the effect of dissolved air on surface heat flux is critical to understanding the general effectiveness of spray cooling using FC-72. For the experiment, data were collected over a range of volume-percent air content of approximately $5 \leq C_m \leq 18\%$, the chamber pressure was maintained nearly constant at $6.90 \times 10^4 \leq P_{ch} \leq 8.27 \times 10^4$ N/m^2 ($10 \leq P_{ch} \leq 12$ psia), and the amount of subcooling ranged from $2 \leq \Delta T_{sc} \leq 12$°C. Each data set contained test runs at flow rates of $\dot{V} = 6.31$, 8.41, and 10.5 cm^3/s (6.0, 8.0, and 10.0 gph); a specified air content by volume C_m; chamber pressure P_{ch}; and fluid subcooling ΔT_{sc}. The percentage of dissolved air by volume in the FC-72 was measured directly using an Aire-Ometer and fluid samples from the test rig, then corrected for experimental conditions using a ratio of partial pressures. An empirical mathematical model was also developed, relating surface heat flux to volumetric flow rate, subcooling, sensible heat, and CHF. The applicability of Henry's law and the use of partial pressures to calculate air concentration was considered and compared with measurements.

Experimental Design and Test Procedure

The test rig used for experimentation was very similar to that described by Baysinger et al. [1], Baysinger [2], and Yerkes et al. [3], but in the current experiment, glass pedestals replaced the polycarbonate pedestals described previously. The stainless steel reservoir in the FC-72 loop was replaced with an acrylic reservoir to allow visualization of the test fluid. Aluminum sumps replaced the polycarbonate sumps used in the initial rig design. The indium-tin oxide heater used previously was replaced with a thick-film resistor heater (for more details, see Puterbaugh [10]).

A spray chamber coupled to a fluid-delivery-loop system made up the two main components of the test rig. The spray chamber was cylindrical, with a cooling jacket surrounding the circular frame. The end caps were fabricated of thick acrylic plates to allow visualization during experimentation. Within the spray chamber, two opposing nozzles allowed fluid to be sprayed onto two opposing thick-film resistor heaters. For the current experiment, only the bottom nozzle was used. The heaters were mounted on glass posts to give structural support and also for insulation to minimize heat loss. A sump system was used to remove excess fluid from around the heaters. To help control spray splashback and guide the working fluid into the sump, angled containment caps were placed over the sump annuli between the spray nozzles and the heater pedestals, partially confining the spray. A circular opening at the top of each cap allowed the spray to enter and contact the heater, but also allowed vapor to freely exit the sump area. The caps were not in contact with the spray nozzles. A wick structure consisting of wire mesh and stainless steel was placed against the inner wall of the cylindrical test chamber to assist with fluid containment. During testing, temperature data were taken using thermocouples embedded within the heater pedestal.

A flow schematic showing each loop and the instruments contained therein can be seen in Fig. 2. One loop was the test-fluid circulation loop, labeled loop A in Fig. 2, which contained the cooling fluid. The FC-72 circulated through the loop and was sprayed from the nozzle onto the heater surface during testing. The second fluid loop, labeled loop B in Fig. 2, was a drain loop for the cooling fluid. The purpose of the drain loop was to remove excess fluid from the spray chamber to ensure that the chamber never became flooded. The third fluid loop, labeled loop C in Fig. 2, contained water, for which the temperature was controlled using reheaters in the loop. The water was circulated around the chamber to control the saturation temperature and pressure of the FC-72 within the chamber. Tubing in low-pressure regions of the fluid loops was composed of plastic, and regions of higher pressure used stainless steel. The system was monitored using a data acquisition system, flow meters, pressure transducers, and type-E thermocouples.

The 0.016-m-diam heater pedestal used in the experiment was similar to that described by Baysinger [2]. However, in the current experiment, a thick-film resistor (TFR) heater was used. A total of five layers of material made up the heater pedestal assembly: the TFR heater, two glass wafers, a glass post, and a glass base. Grooves in the side of the pedestal provided space for thermocouple wires in the various pedestal layers. The heater consisted of a ceramic substrate, a thick-film resistive element, and a glass cover plate. The heater area was 0.00014 m^2. The thicknesses and thermal conductivities of these materials can be seen in Fig. 3. The ceramic substrate formed the base

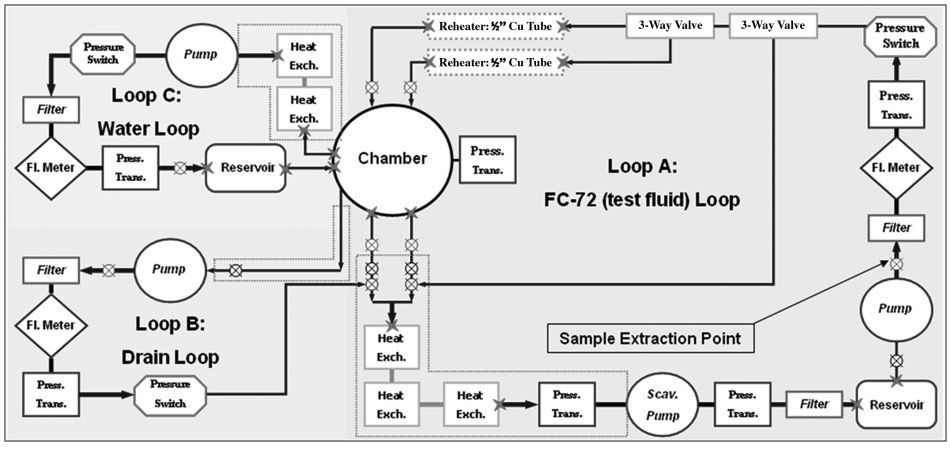

Fig. 2 Flow loop schematic for the experimental test rig.

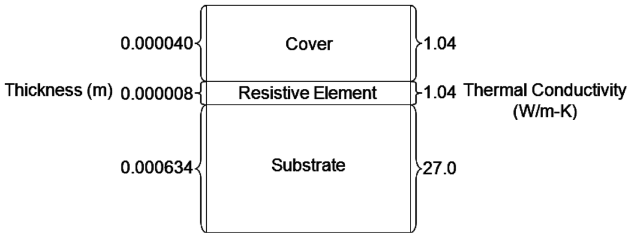

Fig. 3 Heater-layer dimensions and thermal conductivities (not to scale).

of the heater, and the glass cover plate protected the resistive element. The purpose of the glass wafer layers was to allow thermocouple placement at various points in the pedestal.

To control the amount of air contained within the FC-72, several techniques were used. Before the FC-72 loop was filled, the fluid was boiled to remove as much air as possible from the solution, resulting in fluid that was approximately $C = 4\%$ air by volume. The loop was then filled following the fill procedure outlined by Puterbaugh [10]. Following the fill, the amount of dissolved air in the loop fluid was determined via a fluid sample. If the amount of air was greater than desired, a membrane filter (Membrana Superphobic G628) was used to remove air from the FC-72, which consisted of a plastic cylinder with an internal membrane permeable to air, but impermeable to FC-72. If the amount of air in the fluid was less than desired, additional air was bled into the system. The chamber pressure was used as a rough indicator of the amount of air in the system at any given time.

Before each test run, a sample of FC-72 was taken and tested for air content using an Aire-Ometer (Seaton-Wilson AD-4003) with a measurement uncertainty of $\pm 2\%$. These samples were extracted using fill valves downstream of the reservoir. To keep any nonsystem air from being introduced to the sample, the sample line was purged of air and replaced with working fluid. Each sample was then pressure-fed to a hypodermic syringe consisting of approximately 5 ml of fluid. The sample volume was less than 1% of the total fill volume of the spray system. During analysis, 1 ml of the sample was used to flush the Aire-Ometer liquid line. A 1 ml sample was then placed in the Aire-Ometer tube, and the fluid contained within the tube was placed under a slight vacuum, separating the gas contained within the fluid from the fluid itself. Once the gas and fluid were separated, a reading was taken. Three 1 ml samples were analyzed at a given air-content condition to ensure repeatability. Samples were taken and analyzed both before and following a set of test runs, to ensure that the amount of air in the fluid was consistent throughout the entirety of the set. After multiple samples were taken, depleting approximately 20 to 30 ml of fluid volume in the flow loop, the test rig was topped off using additional degassed fluid.

During testing, several experimental parameters were controlled to obtain the desired conditions: the chamber pressure P_{ch}, the amount of subcooling ΔT_{sc}, the volumetric flow rate $\dot{V}$, and the heat rate Q. The chamber pressure was controlled during testing and adjusted if necessary using a reheater incorporated into the water loop. A reheater in the FC-72 loop was used to raise the FC-72 liquid temperature at the nozzle to achieve the desired amount of subcooling. The volumetric flow rate was set to the desired amount and adjusted as necessary throughout the experiment. Once the system was determined to be in equilibrium, the test was started. Voltage to the TFR heater was applied starting at $Q = 5$ W and incrementing the heat input by 5 W every 2 min, allowing the system to reach steady state at each heater increment. Q_{CHF} was defined to be 2.5 W less than the heater power load at which CHF appeared to occur. Such a method for determination of Q_{CHF} was developed to account for the fact that the actual power at which CHF occurred may have been at a level lower than the final power setting, but higher than the previous power setting. Once CHF was reached, the heater power was turned off and the test was terminated.

For data-reduction purposes, it was necessary to determine the surface temperature of the heater. Because no thermocouple was placed on the surface of the heater, no direct method for obtaining the surface temperature existed. As a result, the surface temperature was calculated in terms of the interface temperature using an equation derived from the conservation-of-energy equation along with interface boundary conditions for each of the three heater sections. The geometry of the TFR heater can be seen in Fig. 4. The heat rate produced by the resistive heater is denoted by Q, and f is the fraction of heat rate transferred down the pedestal. The heater was divided into three regions, and each region was analyzed using the conservation-of-energy equation, with the interface fluxes and temperatures as the boundary conditions. Upon integration and application of the boundary conditions, the equation for the surface temperature in terms of the interface temperature is given by [10]

$$T_s = \frac{-(1-f)}{k_{\text{cov}}A} QZ_{\text{cov}} + \frac{QZ_{\text{htr}}}{Ak_{\text{htr}}}\left(f - \frac{1}{2}\right) + T_{\text{int}} + \frac{fQ}{k_{\text{sub}}A} Z_{\text{sub}} \quad (1)$$

Because testing conditions, with the exception of air content, were similar to those used in previous testing by Baysinger et al. [1], Baysinger [2], and Yerkes et al. [3], the value for the amount of heat lost down the pedestal was assumed to be similar. Baysinger et al. [1] initially estimated the heat lost to be approximately 1%, due to the best agreement between transient analytical calculations and experimental results. Baysinger [2] reinforced this estimate, giving a range of 1 to 2.5%. Yerkes et al. [3] again reinforced this estimate through comparison of numerical and analytical solutions for an analysis of the heater and support structure. As a result, the value for f was assumed to be approximately 1.5%, an intermediate value in the previously determined range of 1 to 2.5%.

Upon observation of data obtained through various experimental test runs, it was theorized that an empirical mathematical model for heat flux curves could be developed that would take into account subcooling, sensible heat, CHF, and volumetric flow rate. Heat flux was plotted as a function of wall superheat, which is defined as the temperature drop from the surface of the heater to the saturation temperature $\Delta T = T_s - T_{\text{sat}}$. A second-order mathematical relationship allowing determination of surface heat flux for a given flow rate and surface temperature was developed. Figure 5 shows a theoretical heat flux curve with the key points of interest noted: ΔT_{sc} is the point at which $T_s - T_{\text{sat}} = T_f - T_{\text{sat}}$, $q_{(\Delta T=0)}$ is the heat flux at which saturation temperature is reached, and q_{CHF} and ΔT_{CHF} correspond to the point at which CHF is reached.

To develop the empirical relationship, the surface heat flux q was assumed to be a second-order function of ΔT. Such an assumption was made as a result of the shape of the curve when heat flux was plotted as a function of wall superheat. As a result, the general equation for heat flux was

$$q = a\Delta T^2 + b\Delta T + c \quad (2)$$

The coefficients a, b, and c were determined using ΔT_{sc}, along with the volumetric flow rate $\dot{V}$ and functional relationships for the sensible heat $q_{(\Delta T=0)}$, the critical heat flux q_{CHF}, and the ΔT at which critical heat flux occurs, ΔT_{CHF}. The relationships were developed by plotting each of the three variables, $q_{(\Delta T=0)}$, q_{CHF}, and ΔT_{CHF}, against flow rate for experimental data at three different values for $\dot{V}$. After the plots were made, a second-order polynomial fit was used for each variable to obtain a relationship as a function

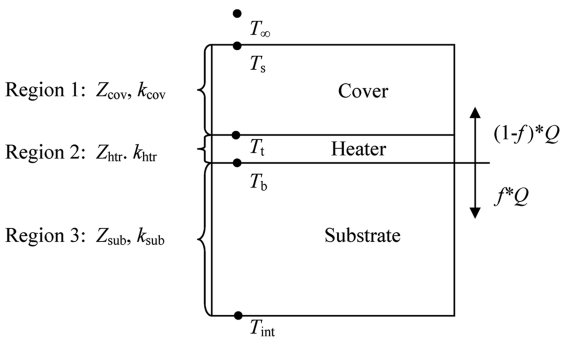

Fig. 4 Thick-film resistor heater schematic (not to scale).

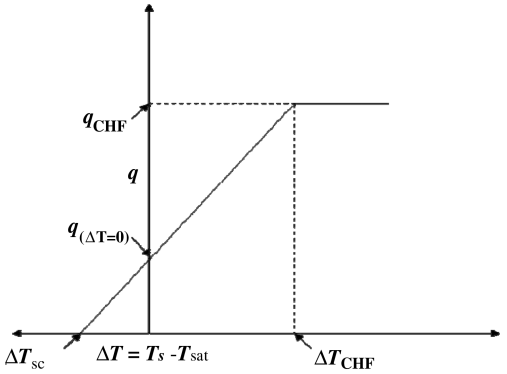

Fig. 5 Typical spray-cooling boiling curve showing key points for coefficient determination.

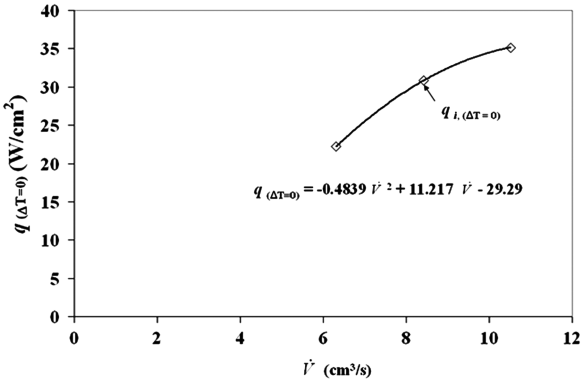

Fig. 6 Functional relationship equations for $q_{(\Delta T=0)}$ at $C_m = 10\%$; $10 \le \Delta T_{sc} \le 12°C$; and $\dot{V} = 6.31$, 8.41, and 10.5 cm^3/s.

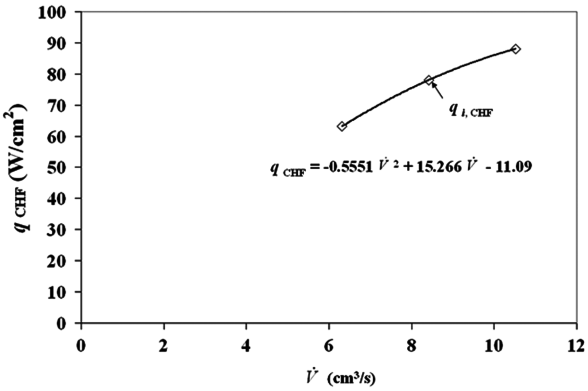

Fig. 7 Functional relationship equations for q_{CHF} at $C_m = 10\%$; $10 \le \Delta T_{sc} \le 12°C$; and $\dot{V} = 6.31$, 8.41, and 10.5 cm^3/s.

of $\dot{V}$. Figures 6–8 show the three functional relationships for $q_{(\Delta T=0)}$, q_{CHF}, and ΔT_{CHF} with volumetric flow rate $\dot{V}$ for the case of $C = 10\%$; $10 \le \Delta T_{sc} \le 12°C$; and $\dot{V} = 6.31$, 8.41, and 10.5 cm^3/s. Following algebraic manipulation, coefficients were determined to be

$$a = -\left\{\frac{q_{(\Delta T=0)}}{\Delta T_{sc}^2} + \left(\left[q_{CHF} + \frac{q_{(\Delta T=0)}\Delta T_{CHF}^2}{\Delta T_{sc}^2} - q_{(\Delta T=0)}\right] \Big/ \Delta T_{sc}\left[\Delta T_{CHF} - \frac{\Delta T_{CHF}^2}{\Delta T_{sc}}\right]\right)\right\} \tag{3}$$

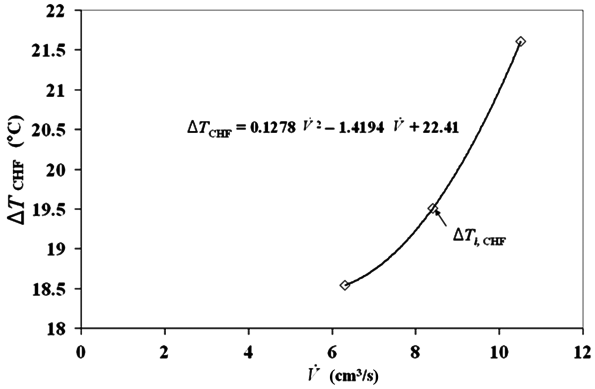

Fig. 8 Functional relationship equations for ΔT_{CHF} at $C_m = 10\%$; $10 \le \Delta T_{sc} \le 12°C$; and $\dot{V} = 6.31$, 8.41, and 10.5 cm^3/s.

$$b = \left\{\left[q_{CHF} + \frac{q_{(\Delta T=0)}\Delta T_{CHF}^2}{\Delta T_{sc}^2} - q_{(\Delta T=0)}\right] \Big/ \left[\Delta T_{CHF} - \frac{\Delta T_{CHF}^2}{\Delta T_{sc}}\right]\right\} \tag{4}$$

$$c = q_{(\Delta T=0)} \tag{5}$$

To make practical use of Eq. (2), a desired flow rate range is chosen. Three tests at identical conditions, with the exception of flow rate $\dot{V}$ are run. One test is run at the upper bound of the flow range, one at the lower bound, and one at a midrange value. Functional relationships for $q_{(\Delta T=0)}$, q_{CHF}, and ΔT_{CHF} are determined from those tests. The relationships are subsequently substituted into Eqs. (3–5), which can then be substituted into Eq. (2), allowing prediction of heat flux curves for varying $\dot{V}$ over the previously specified range.

Results and Discussion

The objective of the current experiment was to determine the effect of dissolved-air content on spray-cooling heat transfer. The dissolved-air volume was measured directly by using an Aire-Ometer. As opposed to direct measurement, work performed by previous researchers has involved determination of dissolved-air amounts using partial pressures and Henry's law. McMurry and Fay [11] stated that the gas solubility of a liquid is proportional to the partial pressure of the gas over the solution:

$$M^* = HP_g \tag{6}$$

where H is Henry's constant and varies depending upon the working fluid and temperature. Henry's law is correctly applied to a closed system in equilibrium. McMurry and Fay [11] described Henry's law and its effects on a system. When a system is at equilibrium at a given pressure, equal numbers of gas particles are entering and leaving the solution. If the pressure in the system is increased, more gas particles are forced to enter the solution than to leave it. With this new equilibrium established, more gas particles are in the liquid than were previously, but the gas particles entering the solution and those leaving are once again equal.

Another notable characteristic of Henry's law is that it is only applicable to dilute gas–liquid solutions. Çengel and Boles [12] characterized dilute gas–liquid solutions as liquids with a small amount of dissolved gas. Unfortunately, a better description of a dilute solution was not found in the archival literature. Çengel and Boles did mention the case of ammonia in water as being one to which Henry's law was not applicable, because ammonia was too soluble in water. According to [13], ammonia is soluble in water up to 31% at 25°C. Also important to note is the temperature dependence of Henry's constant for a given gas–liquid mixture. According to Smith and Harvey [14], Henry's constant has significant nonlinear temperature dependence such that in some cases, a temperature

variation of 10°C can cause a change in Henry's constant by as much as a factor of 2. Henry's constant typically increases with temperature, attains a maximum, and then decreases.

During testing, samples of FC-72 were taken for each data set to determine the air content as a volume fraction, $C_m = [V_{\text{air}}/(V_{\text{FC}} + V_{\text{air}})] \times 100$, and the spray chamber was at saturation conditions with an ambient temperature of $T_{\text{amb}} = 20.5 \pm 0.5$°C. Upon determination of C_m, that value was converted to a volume ratio, $C_m^* = V_{\text{air}}/V_{\text{FC}}$, by the following equation:

$$C_m^* = \frac{(C_m/100)}{1 - (C_m/100)} \tag{7}$$

To implement Henry's law, the volume ratio was converted to a molar ratio, as shown next:

$$M_m^* = C_m^* \left(\frac{\rho_{\text{air,ref}}}{\rho_{\text{FC,ref}}}\right)\left(\frac{m_{\text{FC}}}{m_{\text{air}}}\right) \tag{8}$$

The spray chamber pressure was controlled to maintain a specific saturation temperature during testing. This was done in an attempt to ensure comparability of test results. Although control of the chamber pressure was attempted, identical thermodynamic conditions within the chamber for each test run could not be ensured. As a result, the air content in the fluid being sprayed onto the heater during a test run may have differed from the air content in the fluid being sprayed onto the heater when a fluid sample was taken before testing. A method for obtaining a corrected volume ratio, taking into consideration pressure variations during sampling and testing, was developed. The pressure-corrected volume ratio C^* was obtained using a ratio of Henry's law:

$$M^* = \frac{M_m^* P_g}{P_{g,\text{ref}}} \tag{9}$$

The corrected molar ratio in terms of the corrected volume ratio for the measured values is given by

$$M^* = C^* \left(\frac{\rho_{\text{air}}}{\rho_{\text{FC}}}\right)\left(\frac{m_{\text{FC}}}{m_{\text{air}}}\right) \tag{10}$$

Using Eq. (9) in conjunction with Eqs. (8) and (10), the corrected volume ratio was determined to be

$$C^* = \frac{C_m^* P_g (\rho_{\text{FC}}/\rho_{\text{air}})}{P_{g,\text{ref}}(\rho_{\text{FC,ref}}/\rho_{\text{air,ref}})} \tag{11}$$

Figure 9 shows a typical heater temperature trace with time. Voltage was applied to the TFR heater starting at $Q = 5$ W. The heat input was incremented by 5 W every 2 min, allowing the system to reach steady state at each heater increment. Critical heat flux was considered to have been reached when a dramatic increase in T_{int} indicated loss of sufficient heater cooling, and the temperature cutoff switch on the heater power was triggered when $T_{\text{int}} > 130$°C to prevent damage to the TFR heater. The steady-state increments for several power settings can be seen in Fig. 8, along with the temperature spike indicating CHF.

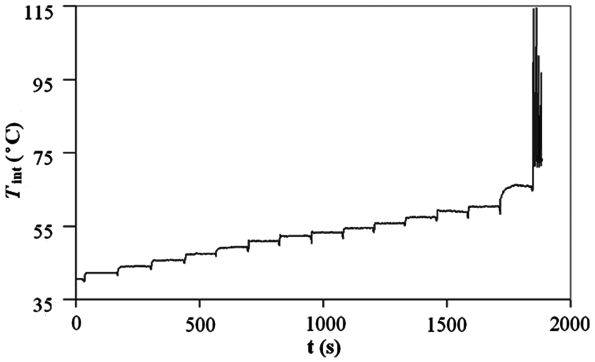

Fig. 9 Heater interface temperature versus time showing several steady states and a CHF event.

To evaluate the effect of varying C on critical heat flux, test runs were grouped according to those with statistically comparable $\dot{V}$, ΔT_{sc}, and P_{ch}. Although statistical comparability was the goal, some of the variables (notably, P_{ch}) were difficult to control. As a result, a few of the parameters in the test cases did not fall within statistical bounds of each other. Groupings were made such that possible trends could be identified. Four sets of three test runs were found to be comparable, as shown in Table 1. Tests conducted with little to no variation in the experimental parameters $\dot{V}$, ΔT_{sc}, P_{ch}, and C_m were seen to yield repeatable results. The heat flux curves in such cases were very similar, and CHF occurred at a similar heat load.

Experimental data showing heat flux curves for each of the data sets in Table 1 can be seen in Figs. 10–13. Note that there was a slight slope change before CHF, to indicate that nucleation was occurring. Each plot shows a distinct heat flux curve for each test run in each set. Comparing all four figures, no trend can be seen with varying C_m. For example, in Fig. 8, the test with the lowest C_m shows the lowest values for q, and in Fig. 9, the test with the highest C_m shows the lowest values for q. Some of the results shown in Table 1 were to be expected. Comparison of sets 1, 3, and 4 shows an increase in CHF with flow rate, as is consistent with previous findings by Estes and Mudawar [15] and Rybicki and Mudawar [16]. Comparison of sets 2 and 3 shows an increase in CHF with subcooling, as is consistent with previous findings by Lin and Ponnappan [6], Horacek et al. [8,9], and Rybicki and Mudawar [16].

It can be seen from Table 1 that no statistical variation in CHF occurred in set 1 of the test runs. Although runs 1a and 1b did not have statistically different air-content values, the air-content value for run 1c was notably higher. From previous research, one would

Table 1 Experimental data sets including precision error only

Run	$\dot{V}$, cm^3/s	ΔT_{sc}, °C	P_{ch}, kPa	C_m, %	C, %	q_{CHF}, W/cm^2
Set 1						
A	6.35 ± 0.07	11.4 ± 0.4	57.8 ± 1.0	8 ± 2	8.04 ± 2.1	65.2 ± 1.8
B	6.28 ± 0.06	11.0 ± 0.4	57.2 ± 1.0	10 ± 2	10.0 ± 2.1	63.4 ± 1.8
C	6.28 ± 0.05	11.3 ± 0.4	72.8 ± 1.0	18 ± 2	18.1 ± 2.2	62.8 ± 1.8
Set 2						
A	8.54 ± 0.13	8.9 ± 0.9	60.1 ± 2.1	5 ± 2	5.1 ± 3.7	69.5 ± 1.8
B	8.50 ± 0.09	10.4 ± 0.8	79.8 ± 2.1	10 ± 2	10.3 ± 3.3	69.3 ± 1.8
C	8.39 ± 0.24	8.2 ± 0.4	80.4 ± 1.2	16 ± 2	16.2 ± 2.1	60.7 ± 1.8
Set 3						
A	8.81 ± 0.15	11.9 ± 0.6	40.3 ± 1.3	5 ± 2	5.0 ± 2.2	71.6 ± 1.8
B	8.37 ± 0.16	11.9 ± 0.5	59.7 ± 1.2	10 ± 2	10.0 ± 2.1	76.8 ± 1.8
C	8.42 ± 0.09	12.2 ± 0.4	76.6 ± 1.1	18 ± 2	18.1 ± 2.2	76.9 ± 1.8
Set 4						
A	10.5 ± 0.06	12.4 ± 0.5	61.2 ± 1.2	8 ± 2	8.0 ± 2.1	91.1 ± 1.8
B	10.4 ± 0.58	12.7 ± 0.4	61.6 ± 1.0	10 ± 2	10.0 ± 2.1	90.6 ± 1.8
C	10.5 ± 0.06	12.8 ± 0.4	79.3 ± 1.2	18 ± 2	18.1 ± 2.2	87.3 ± 1.8

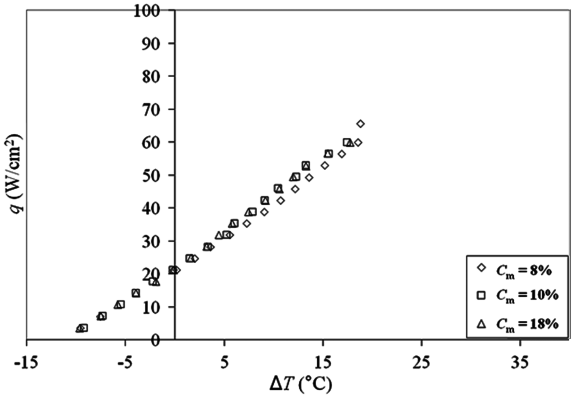

Fig. 10 Heat flux versus wall superheat for various air contents (set 1).

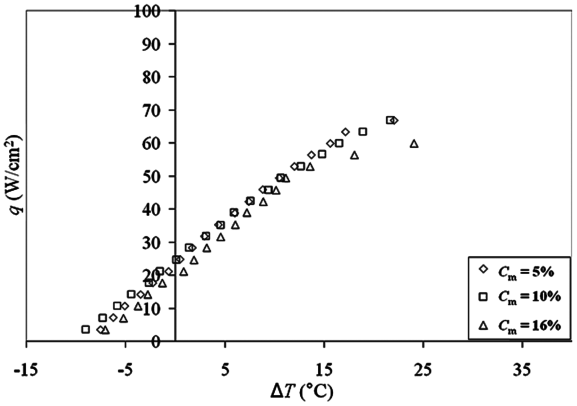

Fig. 11 Heat flux versus wall superheat for various air contents (set 2).

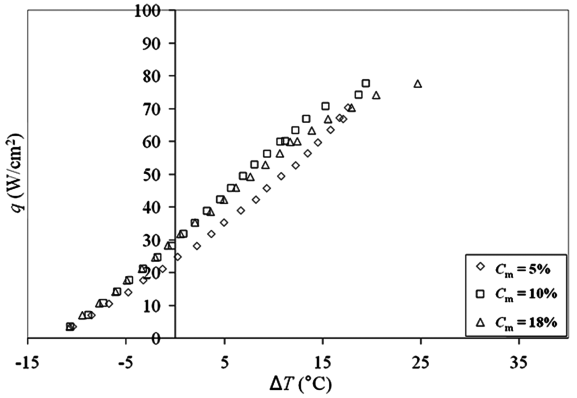

Fig. 12 Heat flux versus wall superheat for various air contents (set 3).

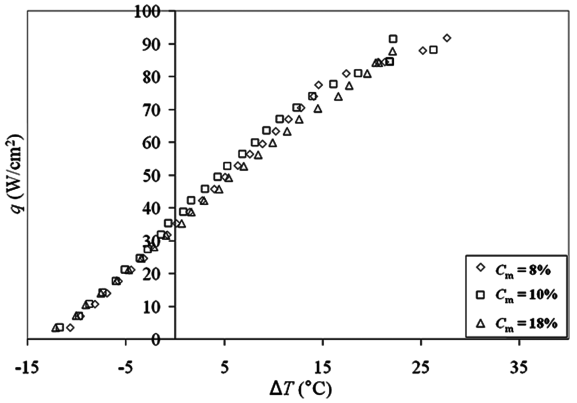

Fig. 13 Heat flux versus wall superheat for various air contents (set 4).

assume that the higher air content would result in a higher CHF [4,7,8]. In fact, the higher P_{ch} value for run 1c would also be expected to cause an increase in CHF. Such a result was not observed. The values for P_{ch} and C increased for each run in set 2, which would be expected to cause consistently increasing values for CHF. Run 2c actually showed a decrease in CHF when compared with runs 2a and 2b, which were statistically similar. A possible explanation for the lower CHF value could be the slightly lower flow rate in run 2c, coupled with a slightly larger than normal error. CHF values for runs 3b and 3c were slightly higher than those for run 3a. The increase between runs 3a and 3b could be explained by the increases in P_{ch} and C. However, P_{ch} and C also increased from run 3b to run 3c, and no corresponding increase in CHF was observed. In set 4, CHF values for runs 4a and 4b were similar, which was to be expected, as they had statistically similar values for C and P_{ch}. In run 4c, however, CHF decreased, which was counterintuitive, as both C and P_{ch} were statistically higher.

There was no significant increase in CHF when P_{ch} was controlled. A possible explanation could be that the air-content values did not cover a sufficiently wide range. In each set of test runs, such an explanation could be considered when comparing run a and run b or run b and run c. However, comparison of run a and run c should include a variation in C large enough to allow observation of effects as a result of that variable. The only case in which the value for q_{CHF} increased for run c when compared with run a was that for set 3. In every other set, the CHF value for run c was either equivalent to or less than that for run a.

The attempt to control P_{ch} could have impacted CHF values and minimized the effect of C. In previous studies, pressure was not controlled, it was simply allowed to vary with air content [6–8]. The attempt at control over that particular parameter could have led to a change in the effect on CHF. Perhaps in previous studies the effect assumed to be caused by variation in C was actually more directly caused by variation in pressure. To determine which variable had a more direct effect on CHF, further investigation would be needed. A set of tests involving constant C values with varying P_{ch} would need to be run and the results compared. If CHF was seen to increase with increasing P_{ch}, it would be reasonable to assume that saturation pressure had more of an effect on critical heat flux than did air content. Figure 14 illustrates the fact that there was no consistent trend in CHF as a function of C.

In an attempt to allow direct comparison between results found in the current research and those found by previous researchers, an effort was made to determine air content using both the Aire-Ometer, with direct fluid samples, and Henry's law, with partial pressures. For each approach, values for M_m^* and M^* were obtained for comparison. Equation (8) was used to calculate M_m^* using C_m^*. The equation for $\rho_{FC,ref}$ was taken from manufacturer information [17], with temperature in °C and density in kg/m^3.

$$\rho_{FC,ref} = 1740 - 2.61(T_{ch,ref}) \tag{12}$$

where $T_{ch,ref}$ was taken as the temperature in the chamber when a fluid

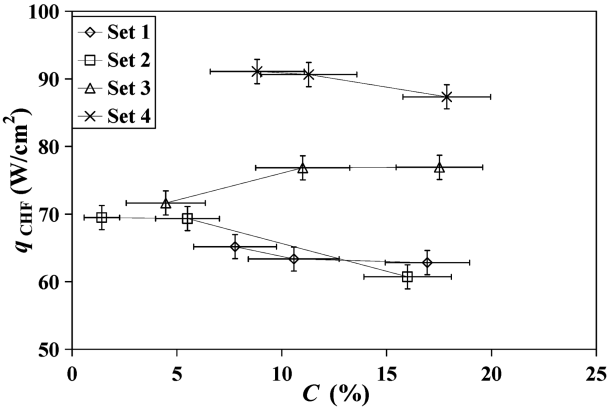

Fig. 14 Critical heat flux versus air content for the four data sets.

sample was taken. The density of air was calculated using the ideal-gas law:

$$\rho_{\text{air,ref}} = \frac{P_{g,\text{ref}}}{RT_{\text{ch,ref}}} \tag{13}$$

The measured partial pressure was determined using the following equation:

$$P_{g,\text{ref}} = P_{\text{tot,ref}} - P_{\text{sat,ref}} \tag{14}$$

where $P_{\text{tot,ref}}$ was taken as the pressure in the chamber when a fluid sample was taken, and $P_{\text{sat,ref}}$ was taken as the vapor pressure corresponding to $T_{\text{ch,ref}}$. The equation for $P_{\text{sat,ref}}$ was taken from FC-72 manufacturer information [17], with temperature in °C and pressure in kPa.

$$P_{\text{sat,ref}} = \frac{(10^{9.729-\frac{1562}{T_{\text{ch,ref}}+273}})}{1000} \tag{15}$$

Equation (10) was used to calculate M^* using C^*, and the equations used to obtain densities and pressures were very similar to Eqs. (12–15) and can be seen next:

$$\rho_{\text{FC}} = 1740 - 2.61T_{\text{ch}} \tag{16}$$

$$\rho_{\text{air}} = \frac{P_g}{RT_{\text{ch}}} \tag{17}$$

$$P_g = P_{\text{tot}} - P_{\text{sat}} \tag{18}$$

$$P_{\text{sat}} = \frac{(10^{9.729-\frac{1562}{T_{\text{ch}}+273}})}{1000} \tag{19}$$

where P_{tot} was the average chamber pressure over the test run, and P_{sat} was the vapor pressure corresponding to T_{ch}, which was the average chamber temperature over the test run.

The measured molar ratio using Henry's law was calculated using a value for Henry's constant for air in FC-72 from Horacek et al. [7]: $H = 5.4 \times 10^{-5}$ mol/mol · kPa for $31°\text{C} < T < 60°\text{C}$. Although the current experimental temperature values fell outside of the temperature range specified, this value was used for calculation purposes because no other value for Henry's constant for air in FC-72 could be found in the archival literature. The equation used to calculate M_m^* using Henry's law can be seen next. Equation (6) was used to calculate M^*:

Table 2 Molar ratio comparison including precision error only

	M^* from C_m^*		M^* from Henry's law	
Run	$M_m^* \times 10^5$	$M^* \times 10^5$	$M_m^* \times 10^5$	$M^* \times 10^5$
Set 1				
a	1.93 ± 0.54	2.02 ± 0.57	146 ± 2	153 ± 6
b	2.24 ± 0.57	2.51 ± 0.60	133 ± 2	150 ± 5
c	7.22 ± 0.71	7.10 ± 0.75	215 ± 2	215 ± 7
Set 2				
a	0.66 ± 0.90	0.24 ± 0.95	80.6 ± 2	30.7 ± 13
b	2.31 ± 0.90	1.65 ± 0.96	133 ± 2	99.9 ± 18
c	5.68 ± 0.67	7.07 ± 0.70	194 ± 2	245 ± 7
Set 3				
a	0.67 ± 0.53	0.56 ± 0.56	84.4 ± 2	71.8 ± 8
b	2.24 ± 0.57	2.73 ± 0.60	133 ± 2	163 ± 6
c	7.22 ± 0.71	7.78 ± 0.75	215 ± 2	235 ± 8
Set 4				
a	1.74 ± 0.54	2.25 ± 0.57	132 ± 2	171 ± 7
b	2.24 ± 0.57	2.91 ± 0.60	133 ± 2	174 ± 6
c	7.22 ± 0.71	8.26 ± 0.75	215 ± 2	249 ± 8

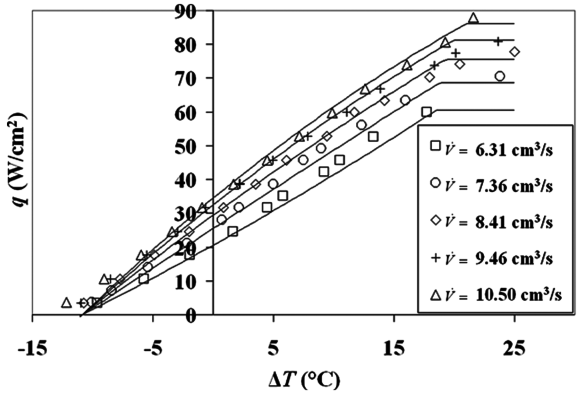

Fig. 15 Heat flux versus wall superheat showing the mathematical model results.

$$M_m^* = HP_{g,\text{ref}} \tag{20}$$

The molar ratios calculated using the measured air content and Henry's law for each test run can be seen in Table 2. The values obtained varied in some cases by an order of magnitude or more. Possible reasons for lack of agreement could include lack of equilibrium and lack of a dilute solution, which were requirements mentioned earlier for applicability of Henry's law. The system used in experimentation had flowing fluid and pressure differences at various points in the fluid loop and thus was inherently not in equilibrium. Also mentioned earlier was the fact that ammonia in water was a solution that was not dilute enough for Henry's law to apply. Air is soluble in FC-72 up to 48% by volume at 25°C [9], which is greater than the 31% solubility of ammonia in water. The fact that air is more soluble in FC-72 than ammonia is in water would indicate that Henry's law may not be applicable to air in FC-72. Another possible reason for the lack of agreement could involve the value used for Henry's constant. The temperatures in the current experiment fall outside the temperature bounds given previously in reference to Henry's constant used for calculation. As a result, the value may not be valid for the current research.

Horacek et al. [7,8] mentioned that although partial pressures were used to calculate the amount of dissolved air in the cooling fluid, nothing could be said about the distribution of air throughout the flowing system at any given time. It may be appropriate to draw a similar conclusion concerning the current experiment, which could also help explain the lack of agreement between values obtained using Henry's law and those using the Aire-Ometer.

The proposed empirical mathematical model was evaluated through comparison of experimental data and predicted data. Experimental data from runs 1b, 3b, and 4b, where $C_m = 10\%$, $10 \leq \Delta T_{\text{sc}} \leq 12°\text{C}$, and $\dot{V} = 6.31$, 8.41, and 10.5 cm^3/s (6.0, 8.0, and 10.0 gph), was used to obtain functional relationships by the method previously discussed. Equation (2), in conjunction with

Table 3 Spray cooling research parameters and results from current data for FC-72

$\dot{V}$, cm^3/s	ΔT_{sc}, °C	P_{ch}, kPa	C_m, %	q_{CHF}, W/cm^2
6.35 ± 0.074	11.4 ± 0.40	57.8 ± 0.97	8 ± 2	65.2 ± 1.8
6.28 ± 0.063	11.0 ± 0.40	57.2 ± 0.97	10 ± 2	63.4 ± 1.8
6.28 ± 0.053	11.3 ± 0.40	72.8 ± 1.0	18 ± 2	62.8 ± 1.8
8.54 ± 0.13	8.91 ± 0.90	60.1 ± 2.1	5 ± 2	69.5 ± 1.8
8.50 ± 0.095	10.4 ± 0.80	79.8 ± 2.1	10 ± 2	69.3 ± 1.8
8.39 ± 0.24	8.22 ± 0.40	80.4 ± 1.2	16 ± 2	60.7 ± 1.8
8.81 ± 0.15	11.9 ± 0.60	40.3 ± 1.3	5 ± 2	71.6 ± 1.8
8.37 ± 0.16	11.9 ± 0.50	59.7 ± 1.2	10 ± 2	76.8 ± 1.8
8.42 ± 0.095	12.2 ± 0.40	76.6 ± 1.1	18 ± 2	76.9 ± 1.8
10.5 ± 0.063	12.4 ± 0.50	61.2 ± 1.2	8 ± 2	91.1 ± 1.8
10.4 ± 0.58	12.7 ± 0.40	61.6 ± 1.0	10 ± 2	90.6 ± 1.8
10.5 ± 0.063	12.8 ± 0.40	79.3 ± 1.2	18 ± 2	87.3 ± 1.8

Table 4 Spray cooling research parameters and results from Lin and Ponnappan [6] for FC-72

$\dot{V}''$, $m^3/m^2 \cdot s$	ΔT_{sc}, °C	Nozzle pressure drop, kPa	C_m, %a	q_{CHF}, W/cm^2
0.0137	Minimized	103	NR	65
0.0167	Minimized	172	NR	72.5
0.0183	Minimized	241	NR	78.5
0.0212	Minimized	310	NR	83.5

[a]NR indicates not reported.

Table 5 Spray cooling research parameters and results from Horacek et al. [7] for FC-72

$\dot{V}$, cm^3/s	$T_{sat} - T_{spray}$, °C	Reservoir pressure, kPa	C_m, %	q_{CHF}, W/cm^2
0.62	2.1	33.4	Degassed	41
0.62	25.7	33.4	Degassed	47
0.62	20.5	67.9	Gaseous	52
0.62	31.7	101	Gaseous	56
0.62	38.6	124	Gaseous	64.5

Table 6 Spray cooling research parameters and results from Horacek et al. [8] for FC-72

$\dot{V}$, cm^3/s	$T_{sat} - T_{spray}$, °C	Reservoir pressure, kPa	C_m, %	q_{CHF}, W/cm^2
0.53	2.1	33.4	Degassed	52
0.53	25.7	33.4	Degassed	45
0.53	20.5	67.9	Gaseous	52
0.53	31.7	101	Gaseous	57
0.53	38.6	124	Gaseous	65

Table 7 Spray cooling research parameters and results from Estes and Mudawar [15] for FC-72

$\dot{V}$, cm^3/s	ΔT_{sc}, °C	Nozzle inlet pressure, kPa	C_m, %a	q_{CHF}, W/cm^2
3.53	33	103	NR	93
5.55	33	103	NR	115
7.57	33	103	NR	136
8.08	33	103	NR	97
12.2	33	103	NR	126
17.3	33	103	NR	166
12.6	33	103	NR	109
18.9	33	103	NR	146
25.2	33	103	NR	177

[a]NR indicates not reported.

Eqs. (3–5) was then used to predict the behavior of surface heat flux at $\dot{V} = 7.36$ and 9.46 cm^3/s (7.0 and 9.0 gph), as shown in Fig. 15. Experimental data are depicted using isolated points, and predicted data are depicted using solid lines. Note that the equation used to determine the predicted data is valid only up to the point at which CHF is reached. Upon reaching CHF, the predicted heat flux value is held constant to depict critical heat flux. As can be seen in the plot, the predicted heat flux compares well with the experimental data.

Conclusions

The effect of dissolved air on the heat transfer performance of a partially confined FC-72 spray was investigated for $5 \leq C_m \leq 18\%$. For the most part, there was no significant variation in heat transfer performance due to varying dissolved air in the spray system when the pressure of the spray chamber was controlled. It was theorized that the effect on CHF attributed by previous researchers to varying air content may have been more directly a result of varying saturation pressure as a result of varying system pressure. Further testing involving constant air content with varying pressure could provide more insight into whether this was indeed the case. If the effect on CHF observed previously was actually a more direct result of system pressure, controlling that pressure could help control CHF, regardless of the amount of air in the system. Tables 3–8 show experimental parameters and results from current and previous research. Observation of gaps in the table, and thus in research to date, could help direct future research efforts. When comparing dissolved-air concentration measurements obtained using fluid samples and those obtained using Henry's law, the results did not agree. The applicability of Henry's law to the current system was found to be questionable due to inherent lack of equilibrium, the possibility that the concentration of air in the working fluid was too high for the solution to be considered dilute, and the use of a possibly incorrect Henry's constant. An empirical mathematical model correlating flow rate, subcooling, sensible heat, and critical heat flux using experimental data was also presented. The model was used to predict the behavior of two test runs and agreed well with experimental data. This may provide a useful, reduced-order empirical approach to model spray-cooling components embedded into system-level thermal management models.

Table 8 Spray cooling research parameters and results from Rybicki and Mudawar [16] for PF-5052

$\dot{V}$, cm^3/s	ΔT_{sc}, °C	Spray chamber pressure, kPa	C_m, %a	q_{CHF}, W/cm^2
3.09	27	101	NR	144
3.54	27	101	NR	155
3.79	27	101	NR	160
9.02	27	101	NR	177
9.99	27	101	NR	194
11.1	27	101	NR	200
12.2	27	101	NR	195
18.5	27	101	NR	210
20.5	27	101	NR	207
3.54	27	101	NR	155
3.54	23	101	NR	144
9.99	27	101	NR	184
9.99	23	101	NR	173
9.99	13	101	NR	128
16.5	27	101	NR	213
16.5	23	101	NR	196
16.5	13	101	NR	137

[a]NR indicates not reported.

Acknowledgment

This research was conducted as part of the in-house program at the U.S. Air Force Research Laboratory, Propulsion Directorate, Power Division, Electrochemistry and Thermal Sciences Branch (AFRL/RZPS), Wright–Patterson Air Force Base, Ohio.

References

[1] Baysinger, K. M., Yerkes, K. L., Michalak, T. E., Harris, R. J., and McQuillen, J., "Design of a Microgravity Spray Cooling Experiment," 42nd AIAA Aerospace Sciences Conference and Exhibit, AIAA Paper 2004-0966, 2004.

[2] Baysinger, K. M., "Experimental Testing and Numerical Modeling of Spray Cooling Under Terrestrial Gravity Conditions," M.S. Thesis, Wright State Univ., Department of Mechanical and Materials Engineering, Dayton, OH, 2005.

[3] Yerkes, K. L., Michalak, T. E., Baysinger, K. M., Puterbaugh, R. L., Thomas, S. K., and McQuillen, J., "Variable-Gravity Effects on a Single-Phase Partially Confined Spray Cooling System," *Journal of Thermophysics and Heat Transfer*, Vol. 20, No. 3, 2006, pp. 361–370. doi:10.2514/1.18681

[4] Milke, J. A., Tinker, S. C., and diMarzo, M., "Effect of Dissolved Gases

on Spray Evaporative Cooling with Water," *Fire Technology*, Vol. 33, No. 2, 1997, pp. 99–113.
doi:10.1023/A:1015386816424

[5] Dawson, H., and diMarzo, M., "Multi-Droplet Evaporative Cooling: Experimental Results," *AIChE Symposium Series*, Vol. 89, No. 295, 1993, pp. 122–131.

[6] Lin, L., and Ponnappan, R., "Heat Transfer Characteristics of Spray Cooling in a Closed Loop," *International Journal of Heat and Mass Transfer*, Vol. 46, No. 20, 2003, pp. 3737–3746.
doi:10.1016/S0017-9310(03)00217-5

[7] Horacek, B., Kim, J., and Kiger, K. T., "Effects of Noncondensable Gas and Subcooling on the Spray Cooling of an Isothermal Surface," ASME International Mechanical Engineering Conference and Exposition, American Society of Mechanical Engineers Paper IMECE-2003-41680, 2003.

[8] Horacek, B., Kim, J., and Kiger, K. T., "Gas Effects on Spray Cooling of an Isothermal Surface: Visualization and Time and Space Resolved Heat Transfer Measurements," 42nd AIAA Aerospace Sciences Meeting and Exhibit, AIAA Paper 2004-1345, 2004.

[9] "Fluorinert^{TM} Electronic Liquids for Electronic Reliability Testing," 3M Specialty Materials, St. Paul, MN, 1999.

[10] Puterbaugh, R., "The Effect of Dissolved Air on the Cooling Performance of a Partially Confined FC-72 Spray," M.S. Thesis, Wright State Univ., Department of Mechanical and Materials Engineering, Dayton, OH, 2008.

[11] McMurry, J., and Fay, R., *Chemistry*, 3rd ed., Prentice–Hall, Upper Saddle River, NJ, 1995, pp. 444–446.

[12] Çengel, Y. A., and Boles, M. A., *Thermodynamics: An Engineering Approach*, 4th ed. McGraw–Hill, New York, 1989, pp. 761–762.

[13] *Spacecraft Water Exposure Guidelines for Selected Contaminants*, Vol 2, National Academy of Sciences, Washington D.C., 2007, p. 39.

[14] Smith, F. L., and Harvey, A. H., "Avoid Common Pitfalls When Using Henry's law," *Chemical Engineering Progress*, Vol. 103, No. 9, 2007, pp. 33–40.

[15] Estes, K. A., and Mudawar, I., "Comparison of Two-Phase Electronic Cooling Using Free Jets and Sprays," *Journal of Electronic Packaging*, Vol. 117, No. 4, 1995, pp. 323–332.
doi:10.1115/1.2792112

[16] Rybicki, J. R., and Mudawar, I., "Single-Phase and Two-Phase Cooling Characteristics of Upward-Facing and Downward-Facing Sprays," *International Journal of Heat and Mass Transfer*, Vol. 49, Nos. 1–2, 2006, pp. 5–16.
doi:10.1016/j.ijheatmasstransfer.2005.07.040

[17] "Fluorinert^{TM} Electronic Liquid FC-72 Product Information," 3M Specialty Materials, St. Paul, MN, 2000.